Prediction-Based Adaptive Control of Haptic Devices Under Communication Time Delay and Human Hand Interference

Khosro Ghorbani Zadeh (IEEE Member), Soroush Izadan, and Saeed Behbahani

***Abstract*—This paper presents a predictor-based adaptive control framework to improve the performance of haptic interaction in the presence of time delay, sampling effects, and uncertain human hand dynamics. In haptic systems, computational delays, zero-order hold effects, and variations in hand impedance can degrade stability and prevent the device from accurately following the continuous trajectory generated by the virtual environment. To address these challenges, the predictor is designed to generate a delay-free trajectory for the adaptive controller, while the adaptive controller estimates uncertain hand impedance parameters and compensates for non-passive forces exerted by the user in real time. To reduce implementation complexity, the effects of sampling and zero-order hold are represented using Taylor series approximations, leading to a more practical theorem for predictor design. The stability of the proposed predictor is established using the linear matrix inequality (LMI) method, and its performance is evaluated in MATLAB/Simulink by comparing it with the widely used Smith predictor.**

***Index Terms*—Haptics, Transparency Improvement, Adaptive Controller, Model-Based Predictors, Time Delay Compensation.**

I. Introduction

As technology continues to advance, the demand for realistic and accurate interaction with virtual objects has steadily increased. Haptic devices play a crucial role in creating immersive experiences by rendering virtual forces and delivering tactile feedback to users. The expansion of this field has led to emerging applications in diverse areas, including science [1], education [2], and daily life, while generating significant economic benefits for manufacturers and service providers.

In haptic interfaces, the system must be controlled not only to maintain stability, which is essential for ensuring the safety of the user or patient, but also to accurately transmit the desired impedance of the virtual environment (VE) to the user. This enables a realistic and believable interaction experience. In this context, transparency is commonly used as a metric that describes the degree of correspondence between the force or sensation actually applied to the user and the force intended by the virtual environment.

Several phenomena can affect the stability and transparency of a haptic system, including time delay, sampling time, quantization, the zero-order hold (ZOH) effect, and the dynamics of the human hand. The impedance properties of the human hand can vary depending on factors such as hand size, orientation, age, and temperature, making it difficult to assign fixed values to hand impedance parameters [3], [4]. The passivity theorem is commonly used to address stability issues in haptic systems [5]. However, this approach has been criticized for neglecting the non passive role of the user's hand and the associated uncertainties. As shown in Table I, human hand impedance parameters can vary substantially across individuals [6].

TABLE I
HAND IMPEDANCE PARAMETERS FOR DIFFERENT USERS [6]

Author	$M_h(Kg)$	$B_h(Ns/m)$	$K_h(N/m)$
Lawrence	17.51	175.1	175.1
Kazerooni	4.54	6.83	12.5
Kousage	1.95	2.46	55
Daniel	1	12.6	39.5
Hogan	0.8	5.5	568
Kuchenbecker	0.15	7.5	1000

Since the human hand is an active dynamic system [4], [7], its time-varying behavior and ability to exert different forces [8] during interaction may reduce the effectiveness of conventional controllers. As a result, the motion of the haptic device and the force feedback transmitted to the user may become unstable or, at best, exhibit significant deviations from the desired values, leading to a loss of interaction transparency. Owing to the uncertainty and variability of hand impedance parameters [9], adaptive control methods can be employed for such systems.

The fundamental concept of adaptive control is to estimate uncertain parameters in real time using measured signals and incorporate these estimates into the control law [10], [11]. Without such adaptation, the system may become inaccurate or unstable due to unmodeled uncertainties. However, the effects of time delay in the virtual environment (VE) are often not considered in adaptive control design, although they may aggravate the parametric uncertainty associated with human hand impedance and the voluntary forces exerted by the user on the haptic device. As discussed earlier, one of

This work is publishing the findings of Khosro Ghorbani Zadeh's Thesis submitted in partial fulfillment of the requirements for the degree of Master of Science at Isfahan University of Technology on November 06, 2021.

Khosro Ghorbani Zadeh was with the Department of Mechanical Engineering, Isfahan University of Technology. He is currently with the Department of Mechanical and Aerospace Engineering, Missouri S&T, Rolla, MO, USA, (email: khosro.ghorbanizadeh@gmail.com)

Soroush Izadan was with the Department of Mechanical Engineering, Isfahan University of Technology, Isfahan, Iran. He is currently with the University of Prince Edward Island, Canada, (email: s.izadan@me.iut.ac.ir)

Saeed Behbahani is with the Department of Mechanical Engineering, Isfahan University of Technology, Isfahan, Iran, (email: behbahani@cc.iut.ac.ir)

the main challenges in maintaining stability and improving the transparency of haptic devices is the high computational burden associated with virtual environment simulations. This computational load can introduce time delay into the system [12], which may degrade transparency. To mitigate this effect, the present study employs a predictor-based approach.

A predictor block, commonly used in teleoperation systems [13], operates in a manner similar to an observer or a Kalman filter. However, unlike conventional state estimators that estimate unmeasured states, a predictor estimates the current value of a known delayed signal and updates this estimate as new measurements become available [13].

The objective of the predictor is to compensate for the effects of time delay and sampling in the virtual environment (VE), thereby enabling the haptic device to follow a continuous trajectory generated by the VE. In [14], a model-based predictor was developed for a nonlinear VE, where Lyapunov–Krasovskii functionals were used to effectively compensate for time-delay effects in VE computations for haptic interaction. However, the time-varying impedance parameters of the human hand and its voluntary force generation were not considered in the model. Moreover, the control law derived from the Lyapunov–Krasovskii framework was relatively complex and difficult to implement in practical scenarios, particularly due to the explicit consideration of sampling time and the zero-order hold (ZOH) model in the theorem. The present study refines the theorem developed in [14] by using Taylor series approximations to represent the effects of sampling and ZOH. This leads to a more practical theorem for predictor design while also incorporating uncertainty in the human hand impedance parameters into the control framework.

Therefore, this research aims to improve the transparency of the haptic system by developing a general control policy that accounts for time delay, sampling effects, and user hand dynamics. The core idea is to design a predictor that generates a delay-free trajectory for the adaptive controller to track. The adaptive controller, equipped with an estimation law, then compensates for the parametric uncertainty of the human hand impedance and the non passive forces exerted by the user while following the predictor trajectory in real time. This enables the user to perceive interactions in the virtual environment more clearly and accurately.

II. System Modeling

A. Haptic Device and User Hand Dynamics

The Cartesian dynamics of the haptic robot can be represented by the following equation:

$$M(x)\ddot{x} + B(x,\dot{x})\dot{x} = F_h + u \tag{1}$$

In this equation, x, $\dot{x}$, and $\ddot{x}$ denote the position, velocity, and acceleration of the haptic interface, respectively. The matrices M and B represent the inertia and damping properties of the system, while u denotes the control input force. Moreover, F_h represents the interaction force exerted between the user and the haptic interface. The validity of this dynamic model has been verified through several experimental studies, such as [15], [16].

Several models have been introduced to describe human hand dynamics during haptic interaction. Among these, a three-parameter linear model has been widely adopted in theoretical analyses [15]–[17], and its accuracy has been validated through experimental investigations, such as [3], [18]. This model can be expressed as:

$$F_h = {F_h}^* - M_h\ddot{x} - B_h\dot{x} - K_h x \tag{2}$$

The interaction force between the user's hand and the haptic interface, denoted by F_h, is modeled as the response of a mass-spring-damper system driven by a bounded external force F_h^*. In this representation, M_h, B_h, and K_h denote the mass, damping, and stiffness parameters of the human hand, respectively. The mass, spring, and damper elements describe the passive mechanical behavior of the user's hand, whereas the external force term represents the voluntary force generated by the user.

By incorporating the human hand dynamics into the dynamic model of the haptic interface, the coupled dynamics of the hand–haptic system can be expressed as:

$$(M + M_h)\,\ddot{x} + (B + B_h)\,\dot{x} + K_h x = {F_h}^* + u \tag{3}$$

The coupled dynamic model of the haptic interface and the user's hand can be reformulated as a linear parameterization of two vectors for implementation in the adaptive controller, as follows:

$$M_s\ddot{x} + B_s\dot{x} + K_s x - {F_h}^* = Y\,(x,\dot{x},\ddot{x})\,\theta \tag{4}$$

In this relation, θ represents the impedance parameters in equation (4), and Y is the position, velocity, and acceleration vector variables. So that:

$$Y\,(x,\dot{x},\ddot{x}) = \begin{bmatrix}\ddot{x} & \dot{x} & x & 1\end{bmatrix}, \theta = \begin{bmatrix}M_s & B_s & K_s & -{F_h}^*\end{bmatrix}^T \tag{5}$$

B. Virtual Tool and Environment Dynamics

The virtual environment can be modeled as a rigid object represented by a mass interacting with its surrounding environment. Alternatively, it may be described using equivalent damping and stiffness elements [14]. In dynamic simulations of haptic interfaces, it is also necessary to include a virtual interaction tool with an associated mass. The dynamics of the virtual object can therefore be expressed as:

$$M_t\ddot{x}_t + B_t\dot{x}_t + K_t x_t = F_h - F_{ve} \tag{6}$$

In this equation, x_t, $\dot{x}_t$, and $\ddot{x}_t$ denote the position, velocity, and acceleration of the virtual tool in the virtual environment, respectively. This tool may be interpreted, for example, as a virtual surgical blade interacting with an organ.

The environment surrounding the tool can be modeled as the portion of the body in contact with the surgical blade, which exerts a reaction force on the tool according to its mechanical stiffness. Similar to physical objects, whose behavior normal to the contact surface can be represented by spring and damping elements, the virtual object can be modeled using a virtual spring with stiffness coefficient K_{ve} and a virtual damper with

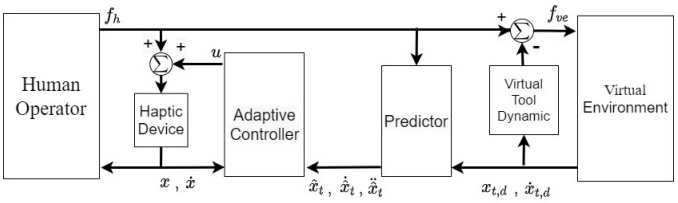

Fig. 1. adaptive control of an admittance-type virtual environment

damping coefficient B_{ve}. Accordingly, the dynamics of the virtual environment can be expressed as follows [19]:

$$F_{ve} = K_w x_t + B_w \dot{x}_t \tag{7}$$

III. Problem Formulation

Figure 1 illustrates the overall schematic of the proposed system. In this system, the human operator interacts with an admittance-type virtual environment (VE) through a haptic device. Since VEs are implemented through computer-based simulations, they are typically represented in the control block design as discrete-time dynamics combined with a time-delay block and a zero-order hold (ZOH). This representation allows the generated trajectory to be reconstructed as a continuous desired path for the haptic device to follow.

Time delays are inevitable in systems involving virtual environments (VEs), and their effects must be addressed within the control loop. In this research, a model-based predictor uses the human force input and the delayed virtual tool position, together with model information, to predict a delay-free trajectory for the controller to track. One advantage of this approach is that the VE design and its stability analysis are separated from the controller design. In other words, as long as the VE remains stable and its stiffness K_{ve} and damping B_{ve} are selected according to appropriate stability criteria, such as those reported in [6] and [19], the controller can be designed independently. Based on the hypothesis presented in [6], this selection implies that the discretization method does not directly affect the stability analysis or predictor design, since K_{ve} and B_{ve} are chosen to ensure stable VE behavior. The overall error is defined as:

$$e = \begin{bmatrix} x - x_t \\ \dot{x} - \dot{x}_t \end{bmatrix} \tag{8}$$

Several criteria have been proposed for evaluating the performance of haptic systems [20]. One widely adopted approach is to minimize the tracking error between the actual trajectory of the haptic interface and the reference trajectory generated by the virtual environment [11], [14]. Therefore, the objective is for the haptic device position, x, to track the virtual tool trajectory, x_t. However, as discussed earlier, VEs are subject to time delays and other anomalies, causing the signal $x_{t,zd}$ to be delay-affected. The goal of this research is to design a predictor capable of estimating a delay-free trajectory, $\hat{x}_t$, and an adaptice controller to follow that.

IV. Controller/Predictor Design

A. Predictor Design

As discussed earlier, the objective of the predictor design is to enable the controller to track a continuous delay-free approximation of the virtual environment (VE) trajectory. In this study, the predictor is designed as a model-based predictor that accounts for the effects of sampling time, time delay, and zero-order hold (ZOH) using the Lyapunov–Krasovskii method.

For time-delay compensation in complex networked and teleoperation systems, the presence of delay makes conventional Lyapunov stability analysis more challenging. Therefore, multivariable coupled inequalities are often required instead of standard Lyapunov-based conditions. These inequalities include decision variables, which can be solved using linear matrix inequality (LMI) techniques. The LMI framework provides an optimization-based approach for finding feasible values of these variables while satisfying the required stability conditions.

The prediction error is defined as the difference between the predicted tool position, $\hat{x}_t$, and the actual delayed tool position, $x_{t,zd}$, which includes the effects of the time delay t_d, sampling, and ZOH.

$$e_{zd} = \begin{bmatrix} \hat{x}_t - x_{t,zd} \\ \hat{x}_t - x_{t,zd} \end{bmatrix} \tag{9}$$

Therefore, the model based predictor's dynamic can be defined as:

$$\begin{aligned} &M_t \ddot{\hat{x}}_t + B_t \dot{\hat{x}}_t + K_t \hat{x}_t = F_h - \hat{F}_{ve} + L e_{z,d} \\ &\hat{F}_{ve} = B_{ve} \dot{\hat{x}}_t + K_{ve} \hat{x}_t \end{aligned} \tag{10}$$

where $L \in \mathbb{R}^{1\times 2}$ denotes the prediction gain. By substituting the virtual environment dynamics into the predictor equation, the following closed-loop dynamics are obtained:

$$\begin{aligned} \dot{e} &= \begin{bmatrix} 0 & 1 \\ -\frac{K_t + K_{ve}}{M_t} & -\frac{B_t + B_{ve}}{M_t} \end{bmatrix} \begin{bmatrix} \tilde{x}_t \\ \dot{\tilde{x}}_t \end{bmatrix} + \begin{bmatrix} 0 \\ \frac{1}{M_t} \end{bmatrix} L e_{z,d} \\ \dot{e} &= Ae + BLe_{z,d} \end{aligned} \tag{11}$$

To develop a systematic method for designing the prediction gain L and proving the closed-loop stability of the predictor in the presence of time delay, ZOH, and sampling effects, the Lyapunov–Krasovskii method is employed. In addition, a Taylor series expansion is used to simplify the stability analysis and obtain a more practical predictor design framework.

Theorem 1: The combined effect of the sampler and ZOH in the virtual environment can be approximated by an equivalent time delay equal to half of the virtual loop sampling period, i.e., $t_d = \frac{T}{2}$.

Proof: The transfer function of the sampler and ZOH in virtual environments is defined as follows [19]:

$$G_{SampleHold}(s) = \frac{1 - e^{-sT}}{sT} \tag{12}$$

Therefore:

$$\begin{aligned} G_{\text{Sample Hold}}(s) &= \frac{1-e^{-sT}}{sT} \\ &\approx \frac{1-\left(1-sT+\frac{s^2T^2}{2}-\frac{s^3T^3}{6}+\cdots\right)}{sT} \\ &= \frac{sT-\frac{s^2T^2}{2}+\frac{s^3T^3}{6}-\cdots}{sT} \\ &\approx e^{-sT/2} \end{aligned} \tag{13}$$

According to [16], separate time delays within a control loop can be combined into an equivalent total delay. Therefore, the total delay present in the virtual environment is given by $t_d + \frac{T}{2}$, where $\frac{T}{2}$ represents the equivalent delay introduced by the sampler and ZOH.

Theorem 2: For the given Non zero scalars a_2, a_3, and $t_d + \frac{T}{2}$, if there exists symmetric positive definite matrices $\bar{P}$, $\bar{Q}$, and $\bar{R}$ as well as matrices $\bar{N}_1$, $\bar{N}_2$, $\bar{N}_3$, Y and a non-singular matrix X such that

$$\begin{bmatrix} \varphi_{11} & \varphi_{21}^T & \varphi_{31}^T & \left(t_d+\frac{T}{2}\right)\bar{N}_1 \\ \varphi_{21} & \varphi_{22} & \varphi_{32}^T & \left(t_d+\frac{T}{2}\right)\bar{N}_2 \\ \varphi_{31} & \varphi_{32} & \varphi_{33} & \left(t_d+\frac{T}{2}\right)\bar{N}_3 \\ \left(t_d+\frac{T}{2}\right)\bar{N}_1^T & \left(t_d+\frac{T}{2}\right)\bar{N}_2^T & \left(t_d+\frac{T}{2}\right)\bar{N}_3^T & -\left(t_d+\frac{T}{2}\right)\bar{R} \end{bmatrix} < 0 \tag{14}$$

where

$$\begin{cases} \varphi_{11} = \bar{Q}+\bar{N}_1+\bar{N}_1^T-AX^T-XA^T \\ \varphi_{21} = \bar{N}_2-a_2AX^T-\bar{N}_1^T-Y^TB^T \\ \varphi_{22} = -\bar{Q}-\bar{N}_2-\bar{N}_2^T-a_2BY-a_2Y^TB^T \\ \varphi_{31} = \bar{P}+\bar{N}_3-a_3AX^T+X \\ \varphi_{32} = -\bar{N}_3-a_3BY+a_2X \\ \varphi_{33} = a_3X^T+a_3X+(t_d+\frac{T}{2})\bar{R} \end{cases} \tag{15}$$

In this case, using a stable gain $L = Y\left(X^T\right)^{-1}$ the system given (11) is stable and the error goes to zero.

Proof: A Lyapunov-Krazuvskii function is chosen as below where P, Q , and R are positive definite matrices $\in \mathbb{R}^{2\times 2}$. Also, the overall system time delay is $t_s = (t_d + \frac{T}{2})$:

$$\begin{aligned} V = e^TPe &+ \int_{t-t_s}^{t} e^T(s)Qe(s)\,ds \\ &+ \int_{-t_s}^{0}\int_{t+\delta}^{t} \dot{e}^T(s)R\dot{e}(s)\,ds\,d\delta > 0 \end{aligned} \tag{16}$$

The Lyapunov derivative is obtained as:

$$\begin{aligned} \dot{V} = \dot{e}^TPe + e^TP\dot{e} + e^TQe - e_s^TQe_s \\ + t_s\dot{e}^TR\dot{e} - \int_{t-t_s}^{t}\dot{e}^T(s)R\dot{e}(s)\,ds \end{aligned} \tag{17}$$

Since the below equation is always right

$$X(t) - X(t-h_1) - \int_{t-h_1}^{t}\dot{X}(s)\,ds = 0 \tag{18}$$

We can derive free matrices $N_i(1,2,3)$ and $M_i(1,2,3)$ such that:

$$\begin{aligned} &\varphi_0 = 2\left(e^TN_1+e_s^TN_2+\dot{e}^TN_3\right)\left(e-e_s-\int_{t-t_s}^{t}\dot{e}(s)\,ds\right) = 0, \\ &\varphi_1 = 2\left(e^TM_1+e_s^TM_2+\dot{e}^TM_3\right)(\dot{e}-Ae-BLe_s) = 0 \end{aligned} \tag{19}$$

By defining $z = \left[e^T\ e_s^T\ \dot{e}^T\right]^T$ as the augmented state variables and adding (19) into (17), the Lyapunov derivative can be represented as

$$\begin{aligned} \dot{V} &= \dot{V} + \varphi_0 + \varphi_1 \\ &= \dot{e}^TPe + e^TP\dot{e} + e^TQe - e_s^TQe_s + t_s\dot{e}^TR\dot{e} \\ &\quad - \int_{t-t_s}^{t}\dot{e}^T(s)R\dot{e}(s)\,ds \\ &\quad + 2z^TN\left[e-e_s-\int_{t-t_s}^{t}\dot{e}(s)\,ds\right] \\ &\quad + 2z^TM\left[\dot{e}-Ae-BLe_s\right] \end{aligned} \tag{20}$$

To further simplify, we can use the following Inequality

$$2z^TN\int_{t-t_s}^{t}\dot{e}(s)\,ds \le t_sz^TNR^{-1}N^Tz + \int_{t-t_s}^{t}\dot{e}^T(s)R\dot{e}(s)\,ds \tag{21}$$

Therefore, the derivative can be minimized to:

$$\begin{aligned} &\dot{V} \le \\ &\dot{e}^TPe + e^TP\dot{e} + e^TQe - e_s^TQe_s^T + t_s\dot{e}^TR\dot{e} + t_sz^TNR^{-1}N^Tz \\ &\qquad + 2z^TN\left[e-e_s\right] + 2z^TM\left[\dot{e}-Ae-BLe_s\right] \end{aligned} \tag{22}$$

The whole derivative can be represented in a matrix inequality form of

$$\dot{V} \le z^T\begin{bmatrix} E_{11} & E_{21}^T & E_{31}^T \\ E_{21} & E_{22} & E_{32}^T \\ E_{31} & E_{32} & E_{33} \end{bmatrix}z + t_sz^TNR^{-1}N^Tz \tag{23}$$

where the elements are

$$\begin{cases} E_{11} = Q+N_1+N_1^T-M_1A-A^TM_1^T \\ E_{21} = -N_1^T+N_2-L^TB^TM_1^T-M_2A \\ E_{22} = -Q-N_2-N_2^T-M_2BL-L^TB^TM_2^T \\ E_{31} = P+N_3+M_1^T-M_3A \\ E_{32} = -N_3+M_2^T-M_3BL \\ E_{33} = M_3+M_3^T+t_sR \end{cases} \tag{24}$$

Applying the Shur Complement [21] results in the integration of the $t_sz^TNR^{-1}N^Tz$ term into the matrix

$$\dot{V} \le z^T\begin{bmatrix} E_{11} & E_{21}^T & E_{31}^T & t_s\bar{N}_1 \\ E_{21} & E_{22} & E_{32}^T & t_s\bar{N}_2 \\ E_{31} & E_{32} & E_{33} & t_s\bar{N}_3 \\ t_s\bar{N}_1^T & t_s\bar{N}_2^T & t_s\bar{N}_3^T & -t_s\bar{R} \end{bmatrix}z \tag{25}$$

This condition describes a non-convex matrix inequality therefore it must be linearized to allow it to be solved using LMI techniques. Therefore, M_2 and M_3 are expressed as scalar mulitples of M_1 (i.e. $M_2 = a_2M_1$ and $M_3 = a_3M_1$). Secondly, the inequality is pre and post multiplied by W and W^T where $W = diag\,(X, X, X, X)$ $\quad, X = M_1^{-1}$. At last, $Y = LX^T$ and $\bar{(.)} = X\,(.)\,X^T$ are defined. The final LMI is given as

$$\begin{bmatrix} \varphi_{11} & \varphi_{21}^T & \varphi_{31}^T & t_s\bar{N}_1 \\ \varphi_{21} & \varphi_{22} & \varphi_{32}^T & t_s\bar{N}_2 \\ \varphi_{31} & \varphi_{32} & \varphi_{33} & t_s\bar{N}_3 \\ t_s\bar{N}_1^T & t_s\bar{N}_2^T & t_s\bar{N}_3^T & -t_s\bar{R} \end{bmatrix} < 0 \tag{26}$$

Where its elements are

$$\begin{cases} \varphi_{11} = \bar{Q} + \bar{N}_1 + \bar{N}_1^T - AX^T - XA^T \\ \varphi_{21} = \bar{N}_2 - a_2 AX^T - \bar{N}_1^T - XL^T B^T \\ \varphi_{22} = -\bar{Q} - \bar{N}_2 - \bar{N}_2^T - a_2 BXL^T - a_2 XL^T B^T \\ \varphi_{31} = \bar{P} + \bar{N}_3 - a_3 AX^T + X \\ \varphi_{32} = -\bar{N}_3 - a_3 BLX^T + a_2 X \\ \varphi_{33} = a_3 X^T + a_3 X + t_s \bar{R} \end{cases} \tag{27}$$

By defining $L = Y\left(X^T\right)^{-1}$, (26) will be simplified to (14). Therefore, if the LMI is solved such that $\bar{P}$, $\bar{Q}$, and $\bar{R}$ are symmetric positive definite and $N_i(1,2,3)$, Y and X exist such that Equation (14) is satisfied that means that $\dot{V} < 0$ and based of the Lyapunov theorem the predictor is stable and even with the existence of a time delay such $t_s = (t_d + \frac{T}{2})$ as the prediction error converges to zero.

B. Controller Design

In this section, an adaptive control law is developed to ensure that the system tracks the delay-free tool trajectory generated by the predictor. The proposed control law is designed to compensate for the uncertain impedance parameters of the human hand. Similar to many dynamic systems with parametric uncertainty, the human hand model includes uncertain impedance values, which are estimated online by the adaptive controller.

The haptic interface uses an encoder to measure the position of the haptic robot manipulated by the operator, while the robot velocity is obtained using numerical differentiation. Acceleration measurements are avoided because numerical differentiation can amplify noise. Therefore, the controller reference signal is selected such that acceleration feedback is not required in the control law. The reference velocity x_r is defined as follows:

$$\dot{x}_r = \dot{x}_t - \Lambda\left(x - x_t\right) \tag{28}$$

In this expression, x_t and $\dot{x}_t$ denote the desired position and velocity obtained from the virtual environment, respectively, and $\Lambda > 0$ is a positive control gain. The objective is to design an appropriate control input, u, such that the velocity of the haptic robot, $\dot{x}$, closely tracks the reference velocity, $\dot{x}_r$. To achieve this objective, the tracking variable s is defined as follows [22]:

$$s = \dot{x} - \dot{x}_r = \dot{x} - \dot{x}_t + \Lambda\left(x - x_t\right) = \dot{\tilde{x}} + \Lambda\left(\tilde{x}\right) \tag{29}$$

The parameter s is directly related to the convergence of $\dot{\tilde{x}}$ and the boundedness of x and $\dot{x}$. Assuming that the initial conditions are bounded, it can be stated that the boundedness of s demonstrates the boundedness of $\tilde{x}$ and $\dot{\tilde{x}}$, and as a result the boundedness of x and $\dot{x}$.

In conclusion, given that specific parameters of the human hand are unknown, the task of designing an adaptive controller is to develop a control law for the control input u and an estimation law for the unknown parameters θ, in order to minimize the error between the haptic robot output and to follow the desired path of the virtual environment x_t. The estimation error is defined as follows:

$$\tilde{\theta} = \hat{\theta} - \theta \tag{30}$$

where θ represents the actual values of the unknown robot parameters and the user's hand, while $\hat{\theta}$ represents their estimated values. To demonstrate stability and derive the appropriate estimation law, a positive definite Lyapunov function is considered:

$$V\left(t\right) = \frac{1}{2} s^T M_s s + \frac{1}{2} \tilde{\theta}^T \Gamma^{-1} \tilde{\theta} > 0 \tag{31}$$

In this relation, $\Gamma = \Gamma^T > 0$ is a positive definite symmetric matrix. Due to the symmetric property of Γ and M_s, The Lyapunov function's derivative will take the following form:

$$\dot{V}\left(t\right) = s^T M_s \dot{s} + \tilde{\theta}^T \Gamma^{-1} \dot{\tilde{\theta}} \tag{32}$$

As mentioned, it is assumed that the impedance parameters of the user's hand are constant in a sampling time, $\dot{\tilde{\theta}} = \dot{\hat{\theta}}$. On the other hand, the system's reference signal can be determined based on the dynamics of the haptic device's interaction with the user's hand.

$$M_s \ddot{x}_r + B_s \dot{x}_r + K_s x - {F_h}^* = Y_r\left(x, \dot{x}, \dot{x}_r, \ddot{x}_r\right)\theta \tag{33}$$

Therefore, the control law can be considered as the following:

$$u = Y_r\left(x, \dot{x}, \dot{x}_r, \ddot{x}_r\right)\hat{\theta} - K_d s \tag{34}$$

This control law includes a parameter estimate of the system's dynamics expressed in terms of reference signal plus a derivative term. By substituting u into the system dynamics and simplifying the equation, we obtain the following closed-loop equation:

$$M_t \dot{s} + \left(K_d + B_s\right) s = Y_r\left(x, \dot{x}, \dot{x}_r, \ddot{x}_r\right)\tilde{\theta} \tag{35}$$

By substituting equation (35) into the Lyapunov function's derivative, the following relationship is obtained:

$$\dot{V}\left(t\right) = -s^T\left(K_d + B_s\right) s + s^T Y_r \tilde{\theta} + \tilde{\theta}^T \Gamma^{-1} \dot{\hat{\theta}} \tag{36}$$

By choosing the estimation rule as:

$$\dot{\hat{\theta}} = -\Gamma {Y_r}^T s \tag{37}$$

The Lyapunov function derivative becomes:

$$\dot{V}\left(t\right) = -s^T\left(K_d + B_s\right) s < 0 \tag{38}$$

We can conclude that V is negative semi-definite since $(K_d + B_s)$ is always positive. V is a positive definite function and $\dot{V}$ is a negative semi-definite function, so according to the Lyapunov's theorem, the closed loop system is stable and the values of s and θ are bounded, but it cannot be concluded that s converges to zero.

To determine that using the proposed control law and estimation law, the closed loop equation of the system converges to zero, Barbalt's lemma is applied. To apply Barbalt's lemma, it is necessary to first demonstrate that $\dot{V}$ is Uniformly

Continuous; for this purpose, it suffices to prove that $\ddot{V}$ is bounded. Using equation (38), we obtain:

$$\ddot{V}(t) = -2{M_s}^{-1} s^T (K_d + B_s) \left(-(K_d + B_s) s + Y_r \tilde{\theta} \right) \tag{39}$$

Considering this equation and the fact that, s and θ are bounded; $\ddot{V}$ is bounded, and thus $\dot{V}$ is uniformly continuous.

Since the Lyapunov function V is positive definite, $\dot{V}$ is semi-definite and uniformly continuous, Barbalt's Lemma concludes that the value of V tends to zero as $t \to \infty$. Consequently, s is also approaching to zero, and as a result of that the values of $\tilde{x}$ and $\dot{\tilde{x}}$ converge toward zero as $t \to \infty$. That means that the adaptive controller tracks $\hat{x}_t$ the predictor generated values.

The presented stability analysis, proves that using the proposed adaptive controller, the haptic device perfectly follows the trajectory of the virtual environment in a stable manner. However, Lyapunov's Theorem and Barbalt's Lemma do not state that θ also converges to zero, but state that θ is bounded. As a result, the adaptation law estimates the values of θ such that $s \to 0$. The tracking does not necessarily converge to zero asymptotically, but depending on the values of K_d, Γ, and Λ, it converges in a finite time despite the hand's parametric uncertainties and the user's interference.

V. Simulation Results

A. Predictors performance

The performance of the predictor is evaluated in two cases. In the first case, only the time delay in the virtual environment is considered, while the effects of the ZOH and sampler are neglected. Under this condition, both stability and performance are analyzed, and an optimization procedure is carried out to determine the optimal predictor gains. In the second case, the effects of the ZOH and sampler are incorporated into the system dynamics, and the resulting model is simulated to evaluate the predictor performance under more realistic conditions.

1) Virtual Environment under time delay: If only time delay is present, the feedback error in can be further defined as:

$$\begin{aligned} M_t \ddot{\hat{x}}_t + B_t \dot{\hat{x}}_t + K_t \hat{x}_t &= F_h - \hat{F}_{ve} + L e_d \\ \hat{F}_{ve} &= B_{ve} \dot{\hat{x}}_t + K_{ve} \hat{x}_t \end{aligned} \tag{40}$$

Here, e_d is used instead of $e_{z,d}$ because only the time-delay effect is present in the control loop. Based on the developed theorem, it can be concluded that the closed-loop dynamics in (40) are stable. Moreover, by selecting an appropriate predictor gain using the MATLAB LMI Toolbox, e_d converges to zero.

To evaluate the performance of the LMI-based predictor, a simulation is conducted in Simulink using the parameters listed in Table II. The human force is defined as $F_h = u(t-1) - 2\sin\left(\frac{t}{\pi}\right)$ to generate a diverse trajectory.

As defined in the theorem, a_2 and a_3 are decision variables whose effects on the prediction error must be investigated. Therefore, an optimization procedure was performed in which the LMI was solved for each combination of (a_2, a_3) using the `feasp` function in MATLAB. For each feasible solution, the corresponding prediction gain L was calculated, as illustrated in Fig. 2. After evaluating several trials, the best values were found at the local minimum corresponding to $a_2 = 0.27$ and $a_3 = 0.01$, resulting in the prediction gain $L = [-114.6563, , -5.2603]$.

TABLE II
Predictor Simulation used Parameters

Parameter	Unit	Value
M_t	[Kg]	35.0
B_t	[Ns/m]	1.0
K_t	[N/m]	82
B_{ve}	[Ns/m]	30
K_{ve}	[N/m]	1000

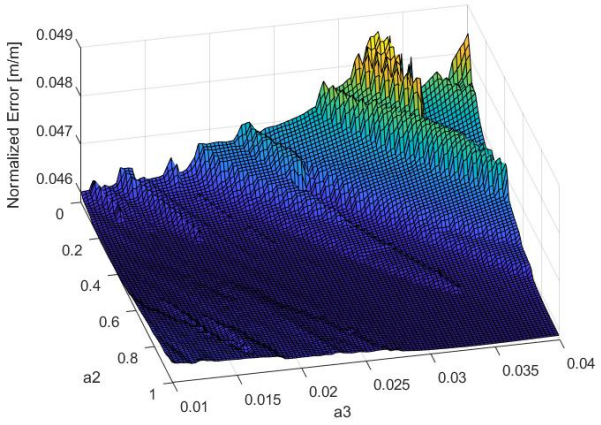

Fig. 2. (a_2, a_3) Predictor Gain Optimization

Using the optimal value of L, the closed-loop predictor dynamics in (40) were simulated, and the resulting position and velocity prediction errors are shown in Fig. 3.

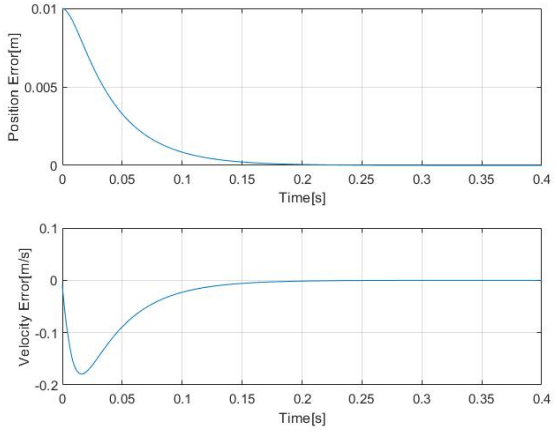

Fig. 3. prediction position and velocity error

As shown in Fig. 3, the predictor accurately tracks the delay-affected virtual position and generates a delay-free trajectory for the controller to follow.

2) Virtual Environment Under Time Delay and Sampling Effects: In the second step, the complete system dynamics

are considered, where the virtual environment is affected by sampling, ZOH, and time delay. The simulation is again performed using the parameters listed in Table II.

By solving the LMI problem, the prediction gain is obtained as $L = [-161.2467, -7.3644]$. This gain is then used in the simulation, and the corresponding predicted and actual position and velocity responses of the virtual tool are shown in Fig. 4.

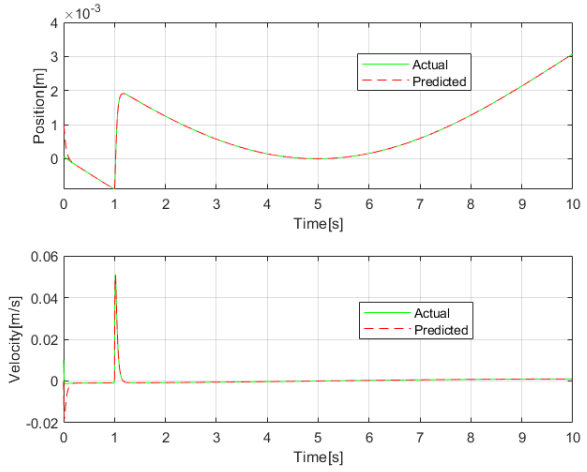

Fig. 4. Virtual tool actual and predicted position and velocity error

As shown in Fig. 4, the predictor accurately tracks the time-delayed virtual environment signal after approximately 200 ms. Fig. 5 illustrates the total error, $e_{z,d}$, associated with the combined effects of time delay and sampling. The predictor rapidly compensates for these effects and generates a corrected trajectory that mitigates the associated anomalies.

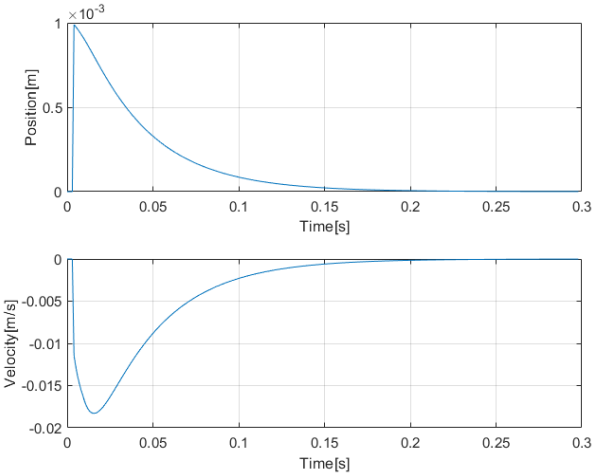

Fig. 5. $e_{z,d}$ total time delay

To further validate the performance of the proposed predictor, it is compared with the well-known Smith predictor. The Smith predictor is commonly designed based on the transfer function of a delay-free system and uses an internal PID control loop with pole-placement techniques to compensate for time delays in physical systems. Fig. 6 shows the block diagram of the Smith predictor designed in this study for the VE connected to the haptic device.

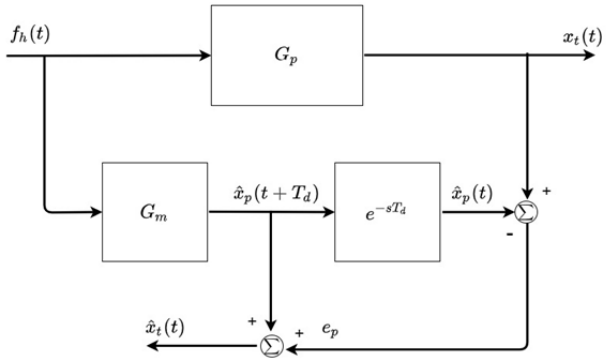

Fig. 6. Smith Predictor

In Fig. 6, G_p represents the transfer function of the virtual environment (VE) with time delay. In this design, the Smith predictor uses the delay-free VE transfer function, G_m, and the known time delay, T_d, to compensate for the delayed real system dynamics represented by G_p. Using the governing equation, the transfer function of the VE and the corresponding block diagram are defined as follows:

$$G_m = \frac{\hat{x}_t(s)}{F_h(s)} = \frac{1}{M_t s^2 + (B_{ve} + B_t)s + (K_{ve} + K_t)} \quad (41)$$

The Smith predictor is simulated using the same parameters listed in Table II, and its predicted position signal is compared with that of the proposed predictor in Fig. 7.

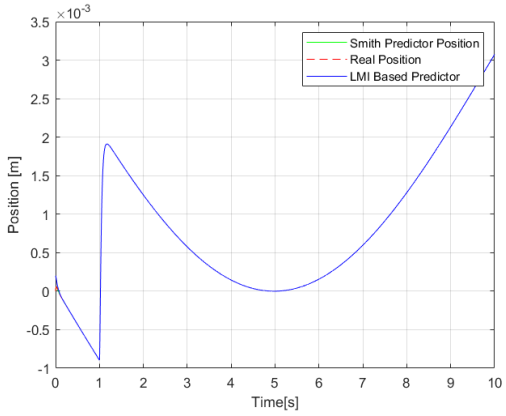

Fig. 7. Smith Predictor and LMI Predictor Performance

As shown in Fig. 7, both predictors effectively compensate for the time delay. However, the Smith predictor exhibits limitations at higher sampling times because its design does not explicitly account for sampling and ZOH effects. Figure 8 presents the simulation results for both predictors with a sampling time of 10 ms.

Based on Fig. 8, it can be concluded that the Smith predictor is unable to adequately compensate for the quantization effects introduced by the sampler and ZOH. If used for trajectory generation in the proposed adaptive controller, this limitation may have detrimental effects because it produces a jerky and nonsmooth reference trajectory for the controller to follow.

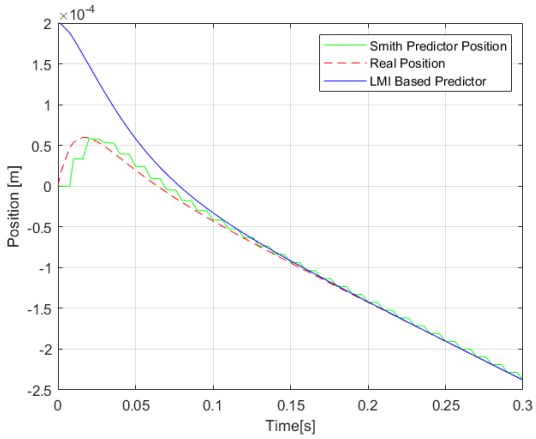

Fig. 8. Smith Predictor and LMI Predictor Performance for higher sampling times

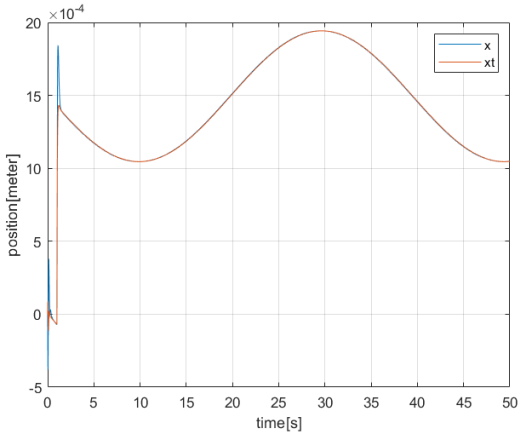

Fig. 9. The position of the haptic device and the virtual tool.

Another limitation of the Smith predictor is its dependence on a known time delay, t_d, which may vary during real-time communication with the VE. In contrast, the LMI-based approach proposed in this research demonstrates greater robustness under varying time-delay conditions due to its gain-scheduling structure.

B. Controller performance

To verify the performance of the designed controller, simulations have been performed in MATLAB. For this purpose, in the Simulink environment, the performance of the haptic device has been investigated for different values of damping and stiffness of the virtual object, as well as for the uncertain parameters of the user's hand. The parameters used in this simulation are shown in Table III. At the same time, the force value of ${F_h}^*$ is equal to $u(t-1)-0.9sin(t/\pi)$ are considered. The quantities M_h, B_h, and K_h in Table III represent the mass,

TABLE III
SIMULATION PARAMETER

Parameter	Value	Parameter	Value
M_t	0.35 Kg	K_{ve}	1000 N/m
B_t	0.1 Ns/m	M_h	4.54 Kg
K_t	82 N/m	B_h	12.5 Ns/m
B_{ve}	30 Ns/m	K_h	6.83 N/m

damping, and stiffness of the user's hand. For this simulation, these values were selected from the test and measurement data for Kazerooni's hand from Table 1. These values are unknown to the controller.

As stated earlier, the purpose of the adaptive controller is to improve the transparency of the haptic device by comparing the actual path followed by the haptic device and the ideal path of the virtual environment. Fig. 9 shows the measured signal for the position of the haptic device and the virtual tool.

As seen in Fig. 9, the position controller's performance is exemplified by its ability to track the haptic device's position in relation to the virtual tool, demonstrating its precision in following the desired path of the virtual environment. Fig. 10 offers a more in-depth look by showing the transient behavior during the initial three seconds of the simulation.

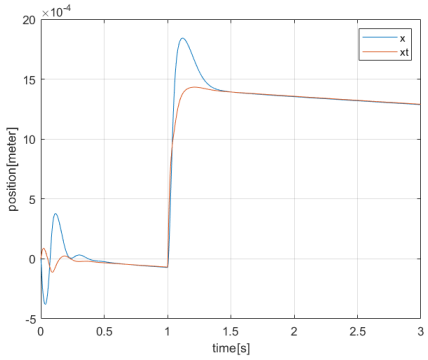

Fig. 10. The position of the haptic device and the virtual tool in the first 3 seconds.

Fig. 10 illustrates the haptic device's ability to closely follow the virtual tool's position with the assistance of the postion controller. The figure highlights two instances of overshoot, the first caused by a parameter mismatch between the controller and the system, and the second resulting from the user's hand's step input in the first second of the simulation. Despite these occurrences, the controller is able to effectively navigate both instances.

Figs. 11 and 12 present the error, as defined by equation (8), which is the difference between the position of the haptic interface and the position of the virtual environment. It is noteworthy that an increase in error corresponds to a decrease in transparency, whereas a decrease in error corresponds to an improvement in transparency.

Fig. 11 depicts reduction in error, indicating a rise in transparency in haptic kinesthetic feedback. Figure 12 examines the associated error between the haptic device's velocity interacting with a hand and the virtual tool's velocity.

As depicted in Fig. 12, the results indicate a close correlation between the velocity of the virtual tool and the haptic device. Furthermore, Fig.13 compares the actual and estimated

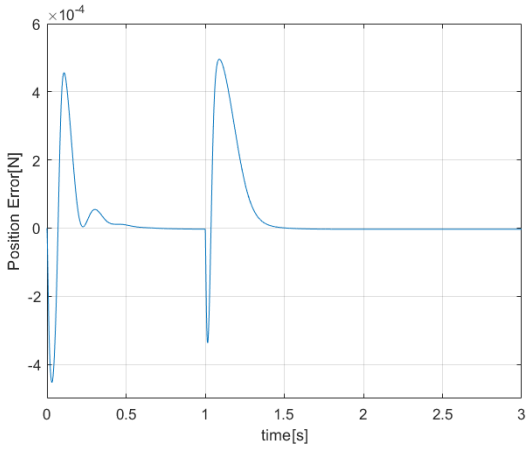

Fig. 11. The position error between the haptic device and the virtual tool.

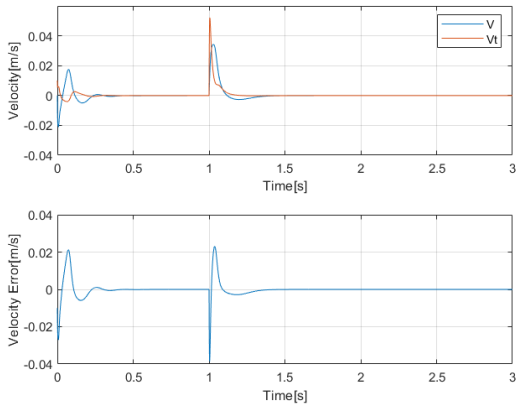

Fig. 12. The velocity of the haptic device and the virtual tool and their associated error.

values for the uncertain parameters, providing further insight into the effectiveness of the adaptive controller.

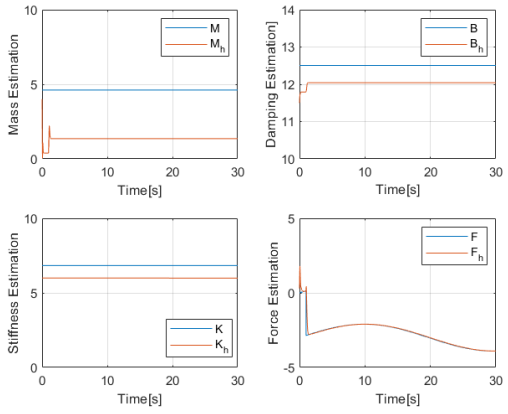

Fig. 13. Estimated values for the uncertain hand parameters.

It can be observed in Fig.13 that $\hat{\theta}$, the estimated values, do not exactly converge to the actual value of θ, and maintain a constant difference throughout the simulation. This difference results from the fact that the Lyapunov Theorem and the Barbalt's lemma did not ensure that $\tilde{\theta}$ will approach zero, but only ensured that it is bounded. Thus, the adapatation law is employed to estimate the values of $\hat{\theta}$ in a manner that guarantees the achievement of the primary objective, which is the minimization of s. This goal is achieved by accurately estimating the haptic device's position.

While alternative adaptive control methods, such as the real-time least squares method, can be used to obtain the uncertain quantities of the system more precisely, they increase the complexity and delay of calculation without being necessary for the achievement of the goal of improving transparency in the presence of uncertainties related to the user's hand impedance. As previously mentioned, the impedance values of the user's hand can vary among individuals, thus, it is important to further investigate the effectiveness of the controller and haptic robot with a diverse range of coefficients and characteristics for impedance. To this end, the quantities of M_h, B_h, and K_h are considered according to the values presented in Table IV, which were selected from the data obtained from the test and measurement for Lawrence's hand as outlined in Table III.

TABLE IV
SIMULATION PARAMETERS FOR LAWRENCE'S HAND

Parameter	Value
M_t	17.5 Kg
B_t	175.1 Ns/m
K_t	175.1 N/m

The decision to use Lawrence's hand quantities in the simulation is based on the fact that they exhibit the most significant deviation from the values examined in the previous section among the available data. As depicted in Fig. 14, the results demonstrate the haptic device's position and the virtual tool's position for the impedance quantities outlined in Table IV.

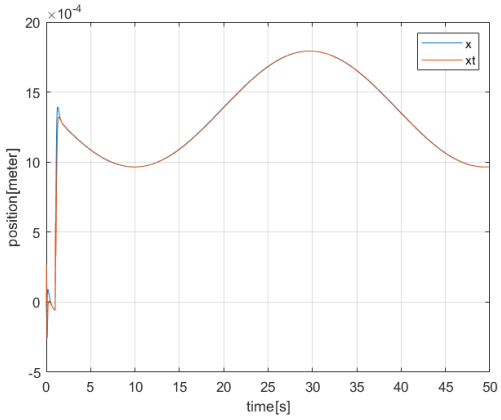

Fig. 14. The position error between the haptic device and the virtual tool for Lawrence's hand.

The results shown in Fig. 14 indicate that the objectives of this research are achieved through the development of an adaptive controller capable of rendering the equivalent impedance of the virtual environment to the user, despite variations in the user's hand parameters. To further validate the effectiveness of the adaptive controller and highlight its

importance, the transparency of the haptic system is also evaluated using a PD controller under uncertain user hand parameters, and the results are compared with those obtained using the adaptive controller.

Figure 15 compares the positions of the haptic device and the virtual tool under the adaptive and PD controllers. It is well established that a PD controller cannot accurately track the virtual tool position when system parameters are uncertain, which leads to reduced transparency in the haptic interface. This behavior is evident from the comparison between the PD controller and the adaptive controller presented in Fig. 15.

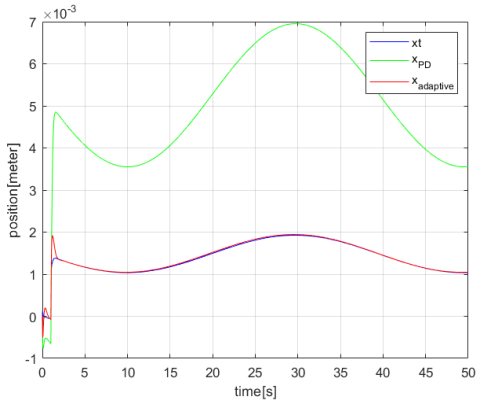

Fig. 15. The comparison of a using PD controller and an Adaptive Controller for motion control of the haptic device.

Fig. 16 examines the first seven seconds of the simulation in greater detail for a better understanding of this phenomenon, emphasizing the importance of using an adaptive controller to improve transparency of haptic interfaces in the presence of dynamic interference from the user's hand.

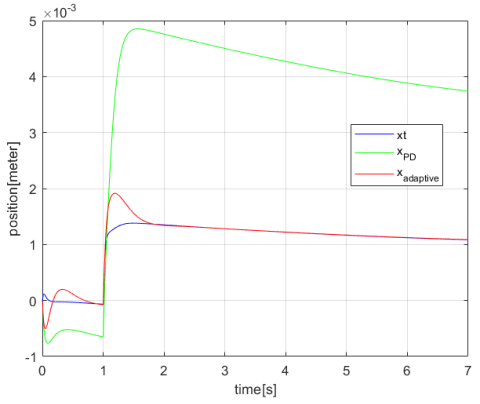

Fig. 16. The comparison of a using PD controller and an Adaptive Controller for motion control of the haptic device for the first 7 seconds.

The comparison between the adaptive controller and the PD controller, shown in Figs. 15 and 16, demonstrates the superior performance of the adaptive controller. This improvement is attributed to its ability to compensate for errors caused by uncertainties in hand parameters, particularly the voluntary force exerted by the user. In contrast, the PD controller cannot account for these uncertainties, resulting in reduced transparency in the haptic interface.

VI. Conclusion

This paper presented a predictor-based adaptive control framework to improve the transparency and stability of haptic interaction in the presence of time delay, sampling effects, ZOH dynamics, and uncertain human hand parameters. A model-based predictor was designed to generate a delay-free trajectory for the adaptive controller, enabling the haptic device to more accurately follow the virtual tool trajectory generated by the virtual environment. To simplify the predictor design and make the stability analysis more practical, the combined effects of the sampler and ZOH were approximated using a Taylor series representation and incorporated into the time-delay model. The stability of the predictor was established through an LMI-based formulation, and the prediction gain was obtained using the MATLAB LMI Toolbox.

Simulation results demonstrated that the proposed predictor effectively compensates for time delay and sampling-related effects, allowing the virtual tool trajectory to be reconstructed smoothly for the controller. Compared with the conventional Smith predictor, the proposed LMI-based predictor showed improved performance under sampling and ZOH effects, particularly at higher sampling times, where the Smith predictor produced nonsmooth trajectory responses. Furthermore, the adaptive controller successfully compensated for uncertainties in the human hand impedance parameters and the voluntary force exerted by the user. Compared with a conventional PD controller, the adaptive controller provided superior tracking performance and improved transparency by reducing errors caused by uncertain hand dynamics. Overall, the proposed framework provides a practical and robust approach for enhancing haptic transparency while preserving stability in delayed and sampled virtual environment interactions.

Acknowledgment

This work is publishing the findings of Khosro Ghorbani Zadeh's Thesis submitted in partial fulfillment of the requirements for the degree of Master of Science at Isfahan University of Technology on November 06, 2021.

References

[1] C. Basdogan, S. De, J. Kim, M. Muniyandi, H. Kim, and M. A. Srinivasan, "Haptics in minimally invasive surgical simulation and training," *IEEE Computer Graphics and Applications*, vol. 24, no. 2, pp. 56–64, 2004.

[2] F. Fazioli, F. Ficuciello, G. A. Fontanelli, B. Siciliano, and L. Villani, "Implementation of a soft-rigid collision detection algorithm in an open-source engine for surgical realistic simulation," in *2016 IEEE International Conference on Robotics and Biomimetics (ROBIO)*. IEEE, 2016, pp. 2204–2208.

[3] N. Hogan, "Controlling impedance at the man/machine interface," in *1989 IEEE International Conference on Robotics and Automation*. IEEE Computer Society, 1989, pp. 1626–1627.

[4] M. M. Beirami, S. Regmi, D. Burns, and Y. S. Song, "Exploring kinematics contribution to the arm stiffness modulation during overground physical human-robot interaction," in *2024 46th Annual International Conference of the IEEE Engineering in Medicine and Biology Society (EMBC)*, 2024, pp. 1–5.

[5] J. E. Colgate and G. G. Schenkel, "Passivity of a class of sampled-data systems: Application to haptic interfaces," *Journal of robotic systems*, vol. 14, no. 1, pp. 37–47, 1997.

[6] A. Mashayekhi, S. Behbahani, F. Ficuciello, and B. Siciliano, "Influence of human operator on stability of haptic rendering: a closed-form equation," *International Journal of Intelligent Robotics and Applications*, vol. 4, pp. 403–415, 2020.

[7] H. Tien, R. Still, K. G. Zadeh, M. M. Beirami, D. Burns, and Y. S. Song, "Development of a force perturbation handle for physical interaction research in humans," *ASME Journal of Biomechanical Engineering*, 2025, under review.

[8] K. G. Zadeh, N. Zendehdel, G. L. Holmes, K. M. Bonnett, A. Costa, D. Burns, M. C. Leu, and Y. S. Song, "Comparison of cnn and lstm networks on human intention prediction in physical human–robot interactions," in *2025 IEEE 21st International Conference on Automation Science and Engineering (CASE)*, 2025, pp. 2408–2413.

[9] M. M. Beirami, S. Regmi, D. Burns, and Y. S. Song, "Understanding human arm stiffness modulation in overground phri: The roles of kinematics, perturbation, and trunk sway," *PLOS ONE*, 2025, under revision.

[10] E. Soleimani, A. K. Sedigh, and A. Nikoofard, "Data-driven reinforcement learning-based forgetting factor iterative learning control," *IEEE Transactions on Automation Science and Engineering*, vol. 22, pp. 12 245–12 256, 2025.

[11] A. Abdossalami and S. Sirouspour, "Adaptive control for improved transparency in haptic simulations," *IEEE Transactions on Haptics*, vol. 2, no. 1, pp. 2–14, 2009.

[12] N. Zendehdel, K. G. Zadeh, H. Chen, Y. S. Song, and M. C. Leu, "Hands-free uav control: Real-time eye movement detection using eog and lstm networks," *IEEE Access*, vol. 13, pp. 101 852–101 868, 2025.

[13] Y.-J. Pan, C. Canudas-de Wit, and O. Sename, "A new predictive approach for bilateral teleoperation with applications to drive-by-wire systems," *IEEE Transactions on Robotics*, vol. 22, no. 6, pp. 1146–1162, 2006.

[14] S. Forbrigger and Y.-J. Pan, "Improving haptic transparency for uncertain virtual environments using adaptive control and gain-scheduled prediction," *IEEE transactions on haptics*, vol. 11, no. 4, pp. 543–554, 2018.

[15] J. J. Gil, A. Avello, A. Rubio, and J. Florez, "Stability analysis of a 1 dof haptic interface using the routh-hurwitz criterion," *IEEE Transactions on Control Systems Technology*, vol. 12, no. 4, pp. 583–588, 2004.

[16] T. Hulin, A. Albu-Schäffer, and G. Hirzinger, "Passivity and stability boundaries for haptic systems with time delay," *IEEE Transactions on Control Systems Technology*, vol. 22, no. 4, pp. 1297–1309, 2013.

[17] K. G. Zadeh and Y. S. Song, "Eso-based adaptive control of haptic devices for transparency improvement and human active force estimation," TechRxiv, Nov. 2025, preprint. [Online]. Available: https://doi.org/10.36227/techrxiv.176300517.79706882/v1

[18] F. A. Mussa-Ivaldi, N. Hogan, and E. Bizzi, "Neural, mechanical, and geometric factors subserving arm posture in humans," *Journal of neuroscience*, vol. 5, no. 10, pp. 2732–2743, 1985.

[19] A. Mashayekhi, S. Behbahani, F. Ficuciello, and B. Siciliano, "Analytical stability criterion in haptic rendering: The role of damping," *IEEE/ASME Transactions on Mechatronics*, vol. 23, no. 2, pp. 596–603, 2018.

[20] I. Desai, A. Gupta, and D. Chakraborty, "Rendering stiff virtual walls using model matching based haptic controller," *IEEE Transactions on Haptics*, vol. 12, no. 2, pp. 166–178, 2019.

[21] S. Boyd, L. El Ghaoui, E. Feron, and V. Balakrishnan, *Linear matrix inequalities in system and control theory*. SIAM, 1994.

[22] J.-J. E. Slotine, W. Li *et al.*, *Applied nonlinear control*. Prentice hall Englewood Cliffs, NJ, 1991, vol. 199, no. 1.